www.czasopisma.pan.pl PAN www.journals.pan.pl

ARCHIVES of FOUNDRY ENGINEERING

DE GRUYTER OPEN

ISSN (2299-2944)
Volume 16
Issue 22016

DOI: 10.1515/afe-2016-0022

Published quarterly as the organ of the Foundry Commission of the Polish Academy of Sciences

33 – 40

Numerical Simulation of Solidification Microstructure based on Adaptive Octree Grids

Y. Yin, Y. Li, K. Wu, J. Zhou*
State Key Laboratory of Materials Processing and Die & Mould Technology,
Huazhong University of Science and Technology, Wuhan 430074, China
*Corresponding author. E-mail address: Zhou Jianxin@hust.edu.cn

Received 24.11.2015; accepted in revised form 19.01.2016

Abstract

The main work of this paper focuses on the simulation of binary alloy solidification using the phase field model and adaptive octree grids. Ni-Cu binary alloy is used as an example in this paper to do research on the numerical simulation of isothermal solidification of binary alloy. Firstly, the WBM model, numerical issues and adaptive octree grids have been explained. Secondary, the numerical simulation results of three dimensional morphology of the equiaxed grain and concentration variations are given, taking the efficiency advantage of the adaptive octree grids. The microsegregation of binary alloy has been analysed emphatically. Then, numerical simulation results of the influence of thermo-physical parameters on the growth of the equiaxed grain are also given. At last, a simulation experiment of large scale and long-time has been carried out. It is found that increases of initial temperature and initial concentration will make grain grow along certain directions and adaptive octree grids can effectively be used in simulations of microstructure.

Keywords: Isothermal solidification, Numerical simulation, Phase field model, Microsegregation, Adaptive octree grids

1. Introduction

Alloy phase field models have been explored by many scholars in the past twenty years. Wheeler, Boettinger and McFadden introduced the phase field model [1,2] for binary alloy firstly in 1992, which is called WBM model. This model is developed by Wheeler and Boettinger [3-5]. Since then, phase field models for treating phase transitions have attracted much interest. In 1997, Braun and Murray improved the phase field of pure metal model and used adaptive finite-difference algorithm to do the simulation [6]. In 1999, Kim gave another phase field model [7,8] by adopting thin interface limit. Boettinger generalized the WBM model, and proposed a model suitable for regular alloy [9] in 2002. Provatas used adaptive mesh refinement to do research on the computation of dendritic microstructures [10-12]. In 2003, Zhao used adaptive finite element method to simulate the growth of directional solidification microstructure [13]. In 2005, Takaki used adaptive quadtree grids to do phase field simulation during directional solidification of binary alloy [14].

2. Mathematical Model

Phase field method is an effective way to simulate the growth of the equiaxed grain. The phase field model in this article is the WBM model proposed by Warren, Boettinger and McFadden. The main equations to be solved are as follows [4,5,7,8] :

$$F=\int_V \left[f(c,\phi,T)+\frac{\varepsilon^2}{2}|\nabla\phi|^2 \right] dV \tag{1}$$

$$\frac{\partial\varphi}{\partial t}=-M_\varphi \frac{\delta F}{\delta\varphi} \tag{2}$$

$$\frac{\partial c}{\partial t} = \nabla \cdot \left[M_c c(1-c) \nabla \left(\frac{\delta F}{\delta c} \right) \right] \tag{3}$$

$$\begin{aligned} f(c,\phi,T) = {} & (1-c) f_A(\phi,T) + c f_B(\phi,T) \\ & + \frac{R_g T}{v_m} \left[c \ln c + (1-c) \ln (1-c) \right] \\ & + c(1-c) \left\{ \Omega_L \left[1 - p(\phi) \right] + \Omega_S p(\phi) \right\} \end{aligned} \tag{4}$$

$$g(\phi) = \phi^2 (1-\phi)^2 \tag{5}$$

$$p(\phi) = \phi^3 \left(6\phi^2 - 15\phi + 10 \right) \tag{6}$$

$$f_A(\phi,t) = W_A g(\phi) + L_A \frac{T_m^A - T}{T_m^A} p(\phi) \tag{7}$$

$$\varepsilon^2 = 6\sigma_A \delta_A \tag{8}$$

$$W_A = 3\frac{\sigma_A}{\delta_A} \qquad W_B = 3\frac{\sigma_B}{\delta_B} \tag{9}$$

$$M_\phi = (1-c) M_\phi^A + c M_\phi^B \tag{10}$$

$$M_\phi^A = \frac{\beta_A T_m^A}{6\delta_A L_A} \qquad M_\phi^B = \frac{\beta_B T_m^B}{6\delta_B L_B} \tag{11}$$

$$M_c = \frac{\left[1 - p(\phi) \right] D_S + p(\phi) D_L}{\left(R_g T / v_m \right)} \tag{12}$$

where ϕ is the phase field taking a value of 0 in the solid and 1 in the liquid, c is the solute concentration, and T is the temperature. $F(c,\phi,T)$ is the volume-free energy, and $f(c,\phi,T)$ is the density of free energy. $f_A(\phi,t)$ and $f_B(\phi,t)$ are the free energy density of the pure components A and B. W_A and W_B are the energy barrier of the pure components A and B. R_g is the gas constant, and v_m is the molar volume. D_L and D_S are the diffusivities in liquid and solid, respectively. σ_A and σ_B are the interfacial energy of pure materials A and B, respectively. β_A and β_B are the kinetic coefficients of pure materials A and B, respectively. T_m^A and T_m^B are the melting points of pure materials A and B, respectively, L_A and L_B are the latent heat of pure materials A and B, respectively, and δ_A and δ_B are the interface thickness of pure materials A and B, respectively Ω_L and Ω_S are the parameters of regular solution, and it is ideal solution when both are equal to 0. Ni–Cu alloy, which is an ideal solution, is used in our simulations, thus Ω_L and Ω_S both are equal to 0.

In practical solidification, the growth of the dendrites are anisotropic and subjected to perturbation. In our simulation, anisotropy is introduced by gradient coefficient of energy as Eq. (13). And Random() whose value is between -1 and 1 is introduced in the left side of Eq. (3) to add perturbation as Eq. (14).

$$W(\mathbf{n}) = \varepsilon_0 \left[1 + \frac{4\varepsilon_4}{1-3\varepsilon_4} \frac{(\partial_x \phi)^4 + (\partial_y \phi)^4 + (\partial_z \phi)^4}{\left| \vec{\nabla} \phi \right|^4} \right] \tag{13}$$

$$\frac{\partial c}{\partial t} \to \frac{\partial c}{\partial t} - \left(16 g(\phi) \right) \chi \, \text{Random}() \tag{14}$$

where ε_0 is constant gradient coefficient of energy, ε_4 is the strength of anisotropy, χ is the strength of noise.

3. Technique of Adaptive Octree Grids

Since one of the advantages of the phase-field method is that the interface position does not have to be explicitly determined, much of the computational work has employed uniform grid techniques. However, it became clear that some type of adaptive technique should be employed in phase-field method to obtain better efficiency. Octree grids are gaining popularity in computational mechanics and physics due to their simple Cartesian structure and embedded hierarchy, which makes mesh adaptation, reconstruction and data access fast and easy. Adaptive octree grid technique is used in the simulation of dendrite growth in our work.

Octree is a way to store three-dimensional data in a tree structure. Each node (cubic grid) in octree has 8 child nodes whose data added together could represent the data of parent node. Meanwhile, each child node could be a father node as it splits into 8 pieces. The layer of the grid is an important parameter which represents the degree of the refinement or coarsening. The larger the layer is, the smaller the grid is, the more the computation is. However, in order to guarantee the precision and save the computing resource, I_{max} and I_{min} are determined and they represent the maximum and minimum layer of grids respectively.

In phase field model, the solid-liquid interface is treated as a certain thickness of the interface and the phase field variables are introduced to track complex interface. The phase field values change continuously near the interfaces, while they take fixed values in the rest of the region. Thus, we focus more on the interfaces in the simulation and the grids of the interfaces are certain to be refined.

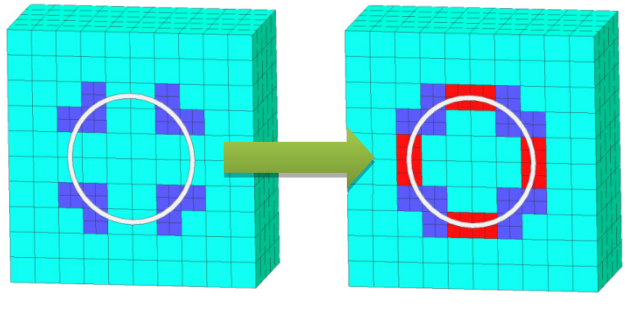

Fig. 1. An example of adaptive octree grids refinement

Figure 1 shows an example of refinement. Assume the white line is the solid-liquid interfaces near which the grids need to be

refined as is shown in red. Adaptive refinement model is proposed here as follows:

$$0 < \phi < 1 \tag{15}$$

$$\begin{cases} fabs(\phi_x) > 0 \\ or \\ fabs(\phi_y) > 0 \\ or \\ fabs(\phi_z) > 0 \end{cases} \tag{16}$$

In this model, all leaf nodes are traversed. If the phase values of the leaf grids are between 0 and 1 or any of the absolute phase field gradient values of the leaf grids along X, Y and Z axes is unequal to zero (namely less than a tiny number in computation), then the grids need to be refined. In the same way, some grids can also be coursing.

The steps of the adaptive grid refinement are as follow:

1) Traversal search each leaf grid, and suppose the leaf cell makes up a set Ω_{leaf}.
2) Judge the phase field value of each leaf cell in the set Ω_{leaf}, the judgment rule is that if the phase field value of the leaf cell is more than 0 and less than 1, defining this cell as a required refine cell and to step 4) ; otherwise, follow the step 3).
3) Calculate the gradient values of the phase field value in the x, y and z directions, if the gradient value of a direction is not 0, defining this cell as a required refine cell and to step 4); if the three values are all 0, follow the step 5).
4) As for the required refine cell in step 2) and 3), if the level of the cell is I_{max} , the cell don not need to be refined; if the level of the cell is less than I_{max}, octree grid refinement technique is adopted to refine the leaf cell and make the level of the cell equal to I_{max}.
5) The refinement of next leaf cell in the set Ω_{leaf} need to repeat step 2) ,until all the leaf cells in the set are refined.

4. Numerical Issues

Initial simulation conditions are shown as follows: the phase field is a sphere whose radius is 8 times the smallest size of mesh. (Assuming that the nucleation of binary alloy has formed a small crystal nucleus), and the sphere is in the centre of the simulation area (the body-centre of the cube), where the phase field value is 0. The phase field value of the rest area is 1. The concentration field value of the nucleation area is 0.3623 (Cu-at) while that of rest area is 0.4083 (Cu-at). The temperature of the computational area is 1356 K. The minimum and maximum layer of the grids is 4 and 8, the minimum size of the mesh is $(\Delta x_{min} \cdot \Delta x_{min})/(10.0 \cdot D_L)$. The boundary conditions are as follows: $\frac{\partial \phi}{\partial n} = 0$, $\frac{\partial c}{\partial n} = 0$ (for all boundaries zero-Neumann boundary condition are imposed.) Parameters of simulation is shown as table 1

Table 1.
Physical parameters of Ni–Cu alloy

parameter symbols	value	parameter symbols	value
T_m^A	1728 K	v_m	$7.43 \cdot 10^{-6}\ m^3/mol$
T_m^B	1000 K	δ_A	$6.11 \cdot 10^{-8}\ m$
D_L	$1.0 \cdot 10^{-9}\ m^2/s$	δ_B	$4.50 \cdot 10^{-8}\ m$
D_S	$1.0 \cdot 10^{-13}\ m^2/s$	σ_A	$0.37\ J/m^2$
β_A	$3.0 \cdot 10^{-3}\ m/(K \cdot s)$	σ_B	$0.39\ J/m^2$
β_B	$3.0 \cdot 10^{-3}\ m/(K \cdot s)$	ε_4	0.05

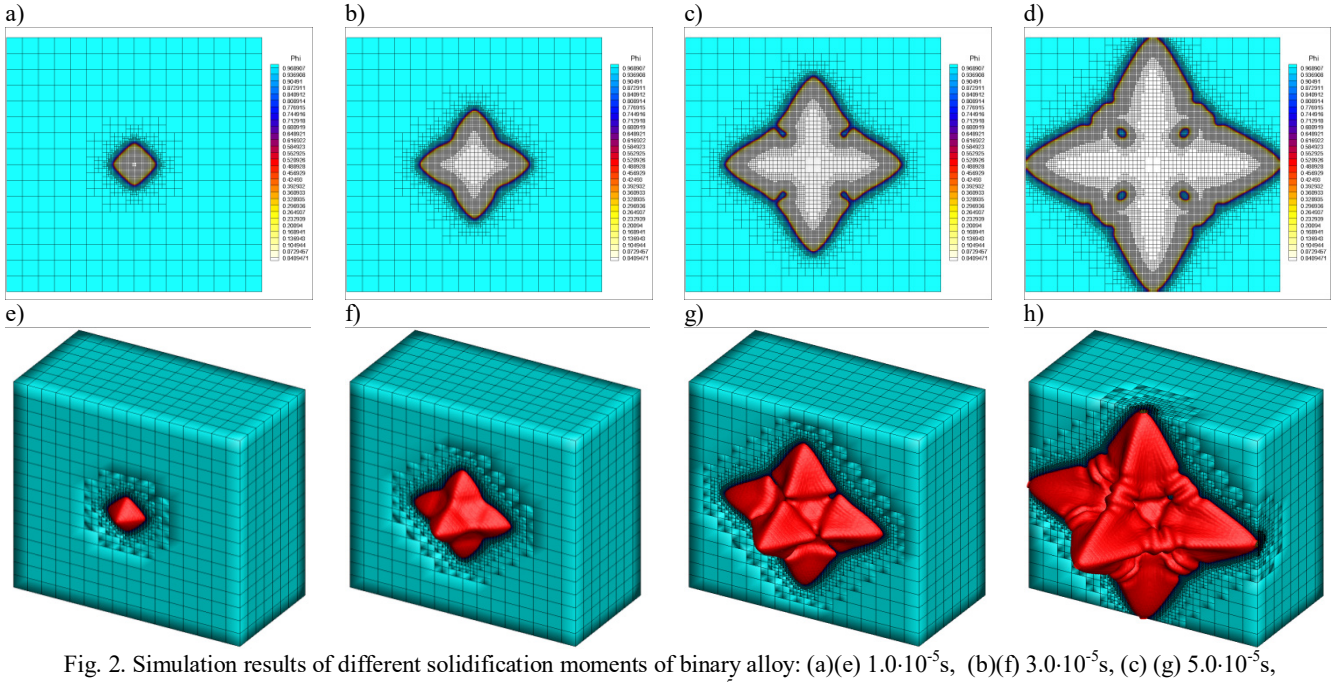

Fig. 2. Simulation results of different solidification moments of binary alloy: (a)(e) $1.0 \cdot 10^{-5}$s, (b)(f) $3.0 \cdot 10^{-5}$s, (c) (g) $5.0 \cdot 10^{-5}$s, (d)(h) $7.5 \cdot 10^{-5}$s

5. Results and Analysis

The computation results are shown as in Figure 2.(a)-(d) are slices which are cut through X-Z plane in the centre of the cube; (e)-(h) are three dimension grids and isosurfaces of 0.5 phase field value. (a) and (e), (b) and (f), (c) and (g), (d) and (h) are simulation results of different moments in the solidification.
The results perfectly illustrate the growth of the equiaxed grain in binary alloy. Firstly, the sphere grain nucleus grows as cellular crystal model. Afterwards, the grain expands quickly along some directions and the grain interfaces concave slowly in the rest area. Concave region can easily be seen in (c) and (g). After formation of concave region, secondary dendrite arms begin to grow in trunk dendrites, the morphology of secondary dendrite arms can also easily be seen in (d) and (h).

5.1. Simulation Results of Concentration Variations

For binary alloy, we pay much attention to composition change as well as to the grain growth morphology. Concentration variations will directly determine the composition distribution of the final binary alloy solidification structure. The simulation results of the grain growth morphology and concentration variations at $6 \cdot 10^{-5}$ s are shown as in Figure 3.(a) and (b) are respectively three-dimensional morphology and two-dimensional slices. It can be seen that solute will accumulate at the interfaces after reaching saturation in solid phase, with the dendrite growth and interface moving in binary alloy solidification. Since the diffusion velocity of the solute in liquid is greater than that in solid (D_L=1.0·10^{-9} m^2/s, D_S=1.0·10^{-13} m^2/s), the diffusion of the solute in liquid will result in concentration gradient of the solute at the interfaces. The diffusivity of the solute in liquid is limited, thus the solute in liquid that is too late to spread will concentrate at the interfaces, namely solute segregation. The concentration variations of the test line A and B (the distance between A and B is 40 times the minimum size of the grid) are plotted in red at Figure 3.(c) and Figure 3.(d) to better analyse simulation results qualitatively. The phase field values are plotted in blue to better illustrate the law of concentration variations.
It can be seen from both curves that there are rises of solute concentration in liquid, which means the closer to the interface, the higher of the solute concentration. The solute concentrations of binary alloy are comparatively lower in solid region. The concentration variations which start at the interfaces are quite small. According to phase field values, it's easy to find that there are peaks of concentration near interfaces in both test lines, which have been analysed previously. The concentration will fall quickly when they comes into solid-liquid interface and reach their minimums in the solid-liquid area. There are also short rising trends before they come into solid. Since the binary alloy in simulation has positive segregation, the solute concentration will decrease rapidly with the increase of the solid fraction, which results in the minimum concentration along with the solute diffusion. However, the further increase of solid fraction will hold up the solute diffusion and leads to the small increase of concentration before they reach solid region. There are declines in the center of both lines. It's because the concentration values has been set quite low in the initial stage of simulation, and the phase field model has adaptive adjustment function, which will gradually adjust the solid solute concentration with calculations going on and lead to increase of solute concentration until reaching the balance. As for test line B, there is a rising crest in solute concentration curve in solid-liquid region. Compare to the two dimensional slice, it's clear to find there are growth areas of secondary dendrites in this place near which are solute enrichment areas.

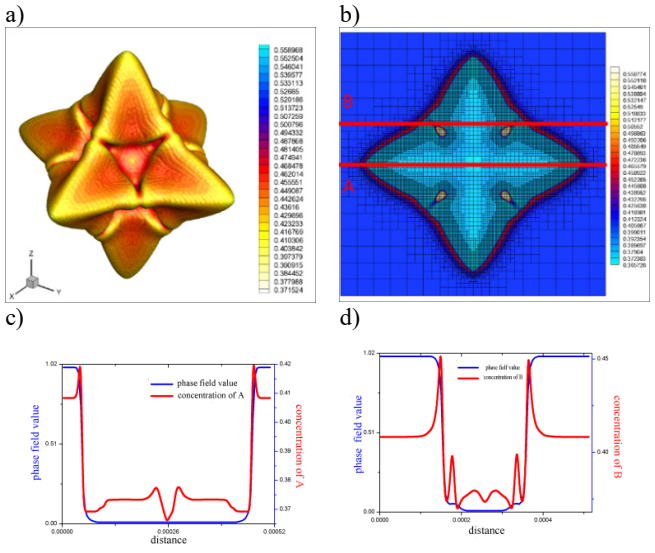

Fig. 3. Concentration variations results of binary alloy: (a) three dimensional morphology; (b) two dimensional slices; (c) results of test line A; (d) results of test line B

5.2. Simulation Results of Microsegregation

It can been seen from previous analysis that interdendritic concentration is high. According to the solute redistribution, much solute will spread into liquid phase and dendritic branches will suppress the solute diffusion during solidification. Thus, microsegregation occurs. In order to describe the degree of microsegregation during solidification of binary alloy, formula (18) is used to indicate the microsegregation:

$$\Omega = \frac{C_{\max}}{C_{\min}} \tag{18}$$

where C_{max} is the maximum amount of component in dendrites, while C_{min} is the minimum amount of component. Results of microsegregation ratio are shown as in Figure 4.

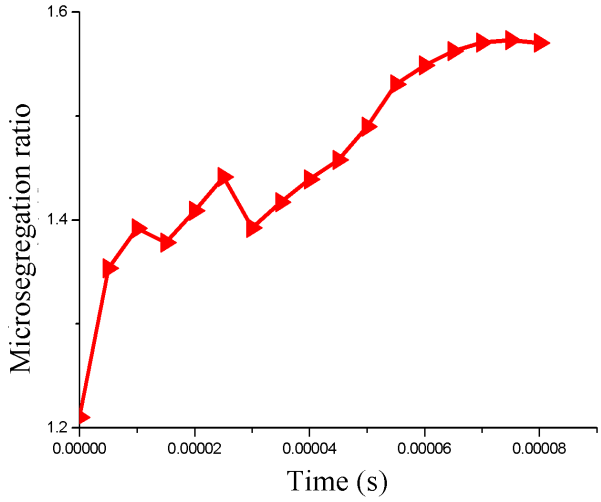

Fig. 4. Microsegregation ratio vs time

The horizontal ordinate is solidification time and vertical coordinate is microsegregation ratio. The microsegregation gradually increases at the beginning of solidification. This is because that the concentration at solid-liquid interfaces is initialized to the fixed value and the concentration of solid is low (alloy of positive segregation), redundant solute in solid will spread into liquid with solidification going on and solid-liquid interface moving. As a result, the microsegregation ratio grows with computation time at the beginning stage of solidification. With solidification continuing, solute accumulation gradually increases, which makes the solute gradient of the of liquid region increase, thus diffusion velocity of the solute in liquid increases. When the diffusion velocity increases to a certain extent, the diffusion of solute in liquid will reach a balance with ejection of solute in solid-liquid region while solidification, the degree of segregation will also reach a balance in this way. It can be seen from the last section of curve that the microsegregation ratio begins to stabilize after $7.0 \cdot 10^{-4}$ s.

In order to better explain the changing law of the concentration field, concentration variations of test line A (namely the fastest growth directions) at different solidification time have been compared in Figure 5.(a)-(d) are slices at different time. The concentration variations at each time have been plotted in the same coordinate system in different color. Figure (e) are basically symmetrical. It can be found the trends of concentration variation near the interfaces at four moment are almost the same, there are all peaks of concentration with basically the same values in four curves. It can be deduced that the maximum concentrations in front of interfaces reach saturation at this moment and the concentration peaks extend outwards with time going on. This agrees with the basic theory of alloy solidification and proves the accuracy of the adaptive octree meshes in the binary alloy solidification simulations. It can also be found there are small fluctuations of concentration at value 0.37 in the solid region. It is because the solute diffusion in solid has been considered in simulation in this paper. Although solute diffusivity of solid is far less than that of liquid, fluctuations still exist as time advances. If concentration fields of solid grids have been ignored, such fluctuations will not exist.

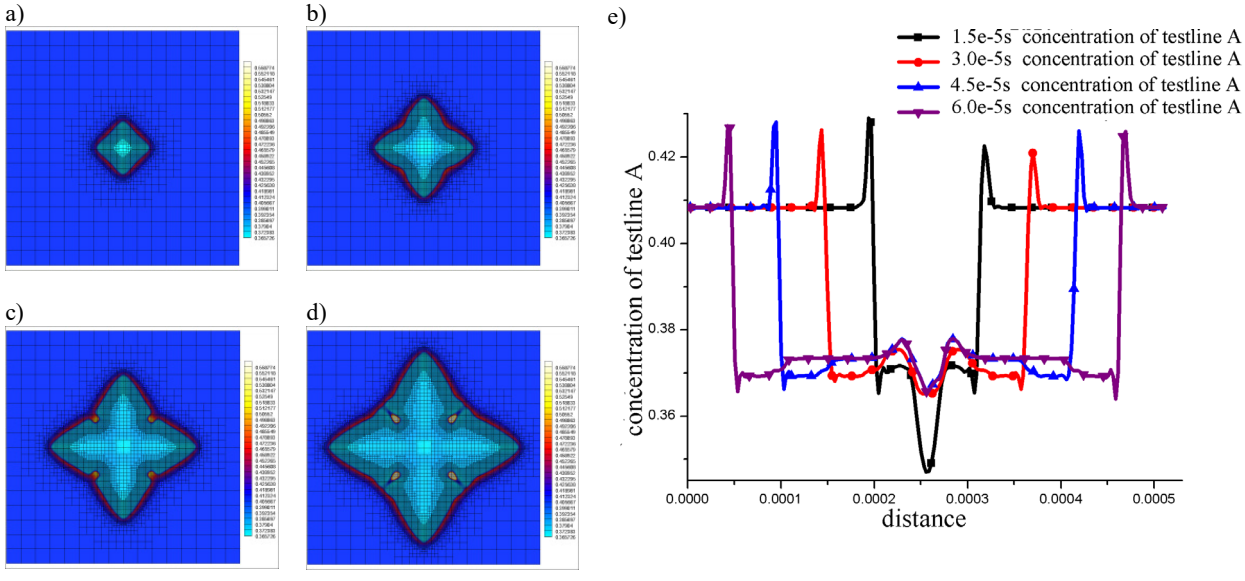

Fig. 5. The concentration variations of test line A at different time: a) $1.5 \cdot 10^{-5}$s, b) $3.0 \cdot 10^{-5}$s, c) $4.5 \cdot 10^{-5}$s, d) $6.0 \cdot 10^{-5}$s, e) concentration variations

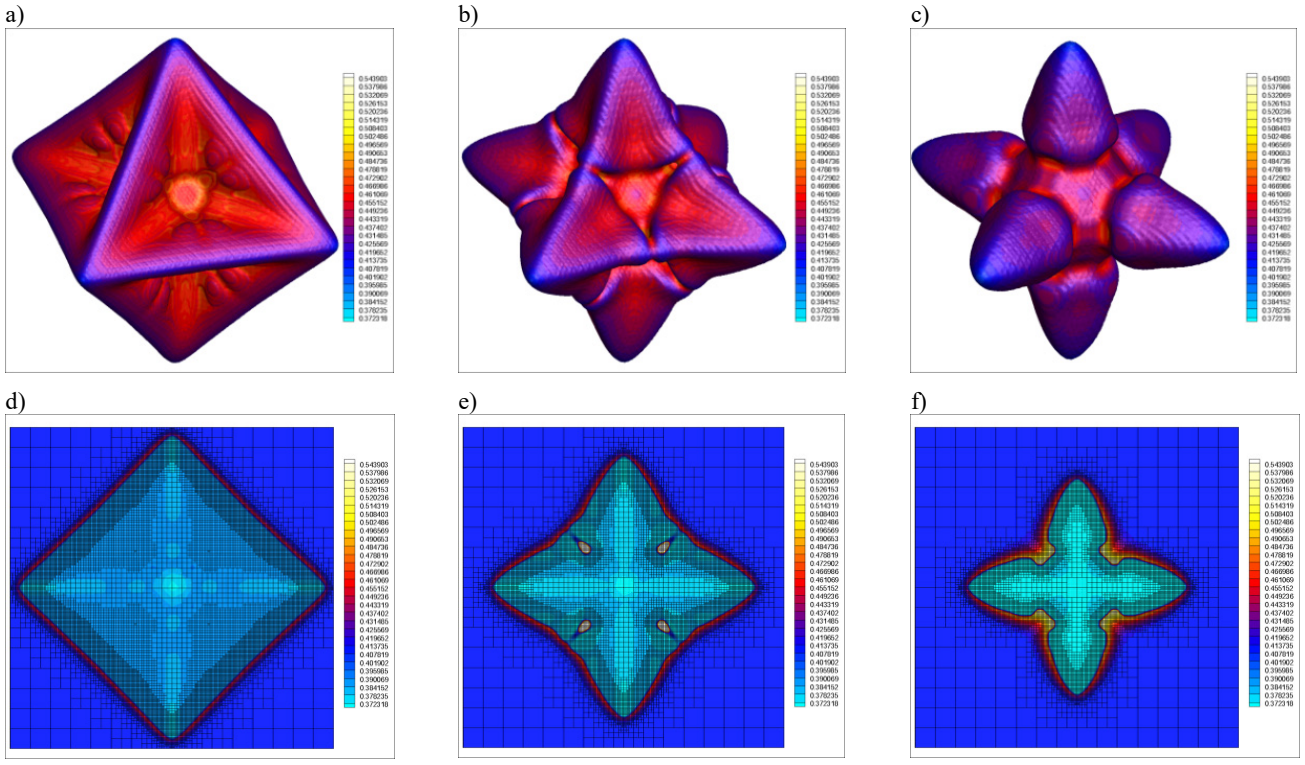

Fig. 6. Results of different initial temperature: a) and d) BE-G1 b) and e) BE-G2 c) and f) BE-G3

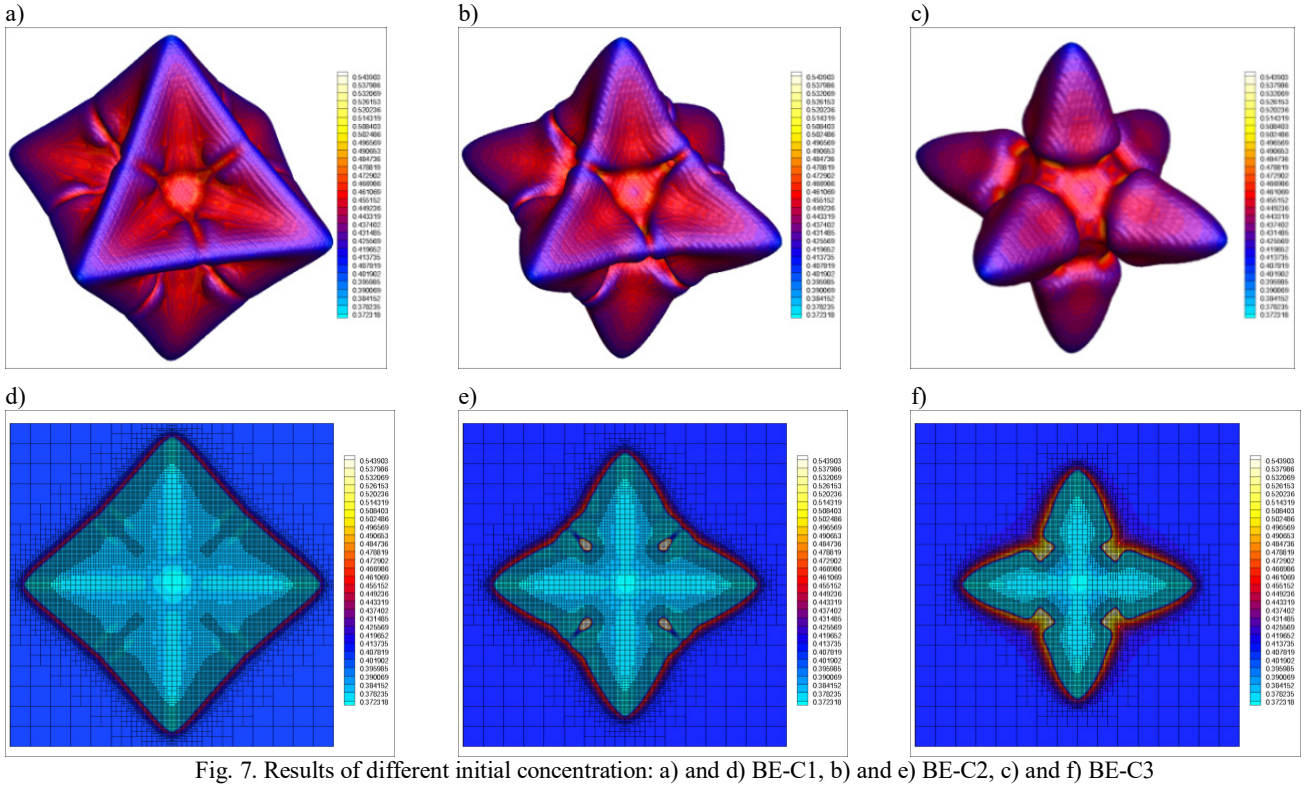

Fig. 7. Results of different initial concentration: a) and d) BE-C1, b) and e) BE-C2, c) and f) BE-C3

Table 2.
The parameter of Ni-Cu alloy under different initial temperature and concentration

Results name	Initial temperature(K)	Initial concentration of Cu(at)
BE-G1	1351	0.4083
BE-G2	1356	0.4083
BE-G3	1361	0.4083
BE-C1	1356	0.4033
BE-C2	1356	0.4083
BE-C3	1356	0.4133

6. The Influence of Physical Parameters on Dendrite Morphology

Since the alloy solidification structures are related to many factors, numerical experiments have been designed in our research to analyse the influence of two parameters on dendrite morphology: initial temperature and initial concentration. Other factors have not been taken into consideration.

6.1. Influence of the initial temperature

The influence of the initial temperature are studied through comparative simulation experiments. The experiments generally apply the same calculating parameters as Table 1. The results of Table 1 of 1356 K initial temperature are named BE-G2. The results of other two experiments whose initial temperature are 1351 and 1361 are respectively named BE-G1 and BE-G3. The simulation results of three-dimensional morphology and two-dimensional slices are shown as Figure 6 when solidification time is $6.0 \cdot 10^{-5}$ s. Color reflects concentration. Three-dimensional morphology are isosurfaces of phase field value at 0.5.

It can be seen from Figure 6 that initial temperature has great influence on morphology of dendrites. In BE-G1, when the initial temperature decreases and undercooling increases, grain grows quickly which can't make solutes spread fully. Thus, grain will grow equally along several growth direction. When the initial temperature increases, undercooling of alloy will reduce, meanwhile, the degree of saturation of alloy will also reduce. Both will result in reduction of the drive force of phase change. At the same time, solutes will spread fully in higher temperature. Thus, the arms of equiaxed dendrite grows quickly. The quick growth of the arms leads to accumulation of solutes near the root of dendrites, which will results in necking phenomenon. And the secondary dendrite arms growth is suppressed.

6.2. Influence of the initial concentration

The influence of the initial concentration are studied through comparative simulation experiments as well. The experiments generally apply the same calculating parameters as Table 1 and Table 2. The results of the experiments, whose initial concentration of Cu is 0.4083, are named BE-C2. The results of other two experiments whose initial concentration (initial concentration of liquid) are 0.005 smaller and larger than BE-C2 are named BE-C1 and BE-C3, respectively. The simulation results of three-dimensional morphology and two-dimensional slices are shown as figure 7 when solidification time is 6.0·10-5 s.

As can be seen in Figure 7, when the initial concentration increases, the constitutional undercooling will decrease. Thus, the driving force of phase transformation will decrease, which results in slow growth of the grain and secondary branches.

7. Simulation Experiment of Large Scale and Long Time

In order to reveal the advantage of adaptive octree grids, a simulation experiment of large scale and long-time has been carried out. In the simulation, the maximum layer of grids is 12, which equals to uniform system of $2^{12} \cdot 2^{12} \cdot 2^{12}$ grids. Ordinary computers can hardly deal with such system. However, it can be perfectly completed with the technique of adaptive octree grids and parallel computation. The result is shown as in Figure 8. It can be seen from the figure that tertiary dendrite arms are quite obvious.

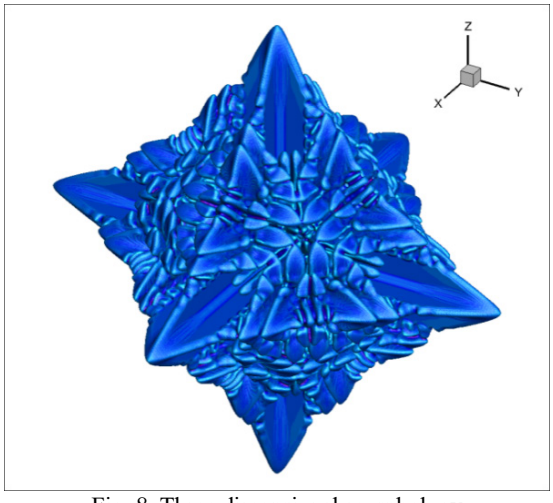

Fig. 8. Three dimensional morphology

8. Conclusions

Adaptive octree mesh computations of solidification of binary alloy have been carried out to simulate the growth of the equiaxed grain in isothermal condition. Three dimensional morphology and

concentration variations are given. It illustrates that the adaptive octree mesh technique can be used in simulation of solidification structure of binary alloy on the premise of precision. And it can effectively save the computing resources and time which will make it advantaged when simulation of alloys with more complex composition are need in the future.

In addition, numerical simulation results of the influence of thermo-physical parameters on the growth of the equiaxed grain are also given in this paper. The initial temperature and initial concentration have great influence on the morphology of the grain. The increases of initial temperature and initial concentration will make grain grow quickly along certain directions. Meanwhile, secondary dendrite arms, even tertiary arms will appear.

Acknowledgments

This research was financially supported by National Natural Science Foundation of China (No.51305149), and National Science & Technology Key Projects of Numerical Control (2012ZX04012-011).

References

[1] Wheeler, A.A., Boettinger, W.J. & McFadden, G.B. (1992). Phase-field model for isothermal phase transitions in binary alloys. *Physical Review A.* 45(10), 7424-7439. DOI: dx.doi.org/10.1103/PhysRevA.45.7424.

[2] Wheeler, A.A., Boettinger, W.J. & McFadden, G. B. (1993). Phase-field model of solute trapping during solidification. *Physical Review E.* 47(3), 1893-1909. DOI: dx.doi.org/10.1103/PhysRevE.47.1893.

[3] Boettinger, W.J. & Warren, J.A. (1996). The phase-field method: simulation of alloy dendritic solidification during recalescence. *Metallurgical and Materials Transactions A*, 27(3), 657-669. DOI: dx.doi.org/10.1007/BF02648953.

[4] Warren, J.A. & Boettinger, W.J. (1995). Prediction of dendritic growth and microsegregation patterns in a binary alloy using the phase-field method. *Acta Metallurgica et Materialia.* 43(2), 689-703.

[5] Boettinger, W.J. & Warren, J.A. (1999). Simulation of the cell to plane front transition during directional solidification at high velocity. *Journal of Crystal Growth.* 200(3), 583-591. DOI: dx.doi.org/10.1016/S0022-0248(98)01063-X.

[6] Braun, R.J. & Murray, B.T. (1997). Adaptive phase-field computations of dendritic crystal growth. *Journal of Crystal Growth.* 174(1), 41-53. DOI: 10.1016/S0022-0248(96)01059-7.

[7] Kim, S.G., Kim, W.T. & Suzuki, T. (1999). Phase-field model for binary alloys. *Physical Review E.* 60(6), 7186-7197. DOI: dx.doi.org/10.1103/PhysRevE.60.7186

[8] Kim, S.G., Kim, W.T. & Suzuki, T. (1998). Interfacial compositions of solid and liquid in a phase-field model with finite interface thickness for isothermal solidification in binary alloys. *Physical Review E.* 58(3), 3316-3323. DOI: dx.doi.org/10.1103/PhysRevE.58.3316

[9] Boettinger, W.J., Warren, J.A., Beckermann, C. & Karma, A. (2002). Phase-field simulation of solidification 1. *Annual Review of Materials Research.* 32(1), 163-194. DOI: 10.1146/annurev.matsci.32.101901.155803.

[10] Provatas, N., Goldenfeld, N. & Dantzig, J. (1998). Efficient computation of dendritic microstructures using adaptive mesh refinement. *Physical Review Letters.* 80(15), 3308-3311. DOI: dx.doi.org/10.1103/PhysRevLett.80.3308.

[11] Provatas, N., Goldenfeld, N. & Dantzig, J. (1999). Adaptive mesh refinement computation of solidification microstructures using dynamic data structures. *Journal of Computational Physics*. 148(1), 265-290. DOI: 10.1006/jcph.1998.6122.

[12] Provatas, N., Greenwood, M., Athreya, B., Goldenfeld, N. & Dantzig, J. (2005). Multiscale modeling of solidification: phase-field methods to adaptive mesh refinement. *International Journal of Modern Physics B,* 19(31), 4525-4565. DOI: 10.1142/S0217979205032917.

[13] Zhao, P., Vénere, M., Heinrich, J.C. & Poirier, D.R. (2003). Modeling dendritic growth of a binary alloy. *Journal of Computational Physics*. 188(2), 434-461.

[14] Takaki, T., Fukuoka, T. & Tomita, Y. (2005). Phase-field simulation during directional solidification of a binary alloy using adaptive finite element method. *Journal of Crystal Growth*. 283(1), 263-278. DOI: 10.1016/j.jcrysgro.2005.05.064.